Inorganic Chemistry

ARTICLE

pubs.acs.org/IC

Ruthenium Complexes Containing 2-(2-Nitrosoaryl)pyridine: Structural, Spectroscopic, and Theoretical Studies

Siu-Chung Chan, Ho-Yuen Cheung, and Chun-Yuen Wong*

Department of Biology and Chemistry, City University of Hong Kong, Tat Chee Avenue, Kowloon, Hong Kong SAR, People's Republic of China

Supporting Information

ABSTRACT: Ruthenium complexes containing 2-(2-nitrosoaryl)-pyridine (ON^N) and tetradentate thioether 1,4,8,11-tetrathiacyclotetradecane ([14]aneS4), [Ru(ON^N)([14]aneS4)]$^{2+}$ [ON^N = 2-(2-nitrosophenyl)pyridine (**2a**), 10-nitrosobenzo[*h*]quinoline (**2b**), 2-(2-nitroso-4-methylphenyl)pyridine, (**2c**), 2-(2-nitroso-phenyl)-5-(trifluoromethyl)pyridine (**2d**)] and analogues with the 1,4,7-trithiacyclononane ([9]aneS3)/*tert*-butylisocyanide ligand set, [Ru(ON^N)([9]aneS3)(C≡N^{t}Bu)]$^{2+}$ (**4a** and **4b**), have been prepared by insertion of a nitrosonium ion (NO$^+$) into the Ru−aryl bond of cyclometalated ruthenium(II) complexes. The molecular structures of the ON^N-ligated complexes **2a** and **2b** reveal that (i) the ON^N ligands behave as bidentate chelates via the two N atoms and the bite angles are 86.84(18)−87.83(16)° and (ii) the Ru−N_{NO} and N−O distances are 1.942(5)−1.948(4) and 1.235(6)−1.244(5) Å, respectively. The Ru−N_{NO} and N−O distances, together with $\nu_{N=O}$, suggest that the coordinated ON^N ligands in this work are neutral moiety $(ArNO)^0$ rather than monoanionic radical $(ArNO)^{\bullet-}$ or dianion $(ArNO)^{2-}$ species. The nitrosated complexes **2a**−**2d** show moderately intense absorptions centered at 463−484 nm [ε_{max} = (5−6) × 10^3 dm^3 mol^{-1} cm^{-1}] and a clearly discriminable absorption shoulder around 620 nm (ε_{max} = (6−9) × 10^2 dm^3 mol^{-1} cm^{-1}), which tails up to 800 nm. These visible absorptions are assigned as a mixing of d(Ru) → ON^N metal-to-ligand charge-transfer and ON^N intraligand transitions on the basis of time-dependent density functional theory (TD-DFT) calculations. The first reduction couples of the nitrosated complexes range from −0.53 to −0.62 V vs $Cp_2Fe^{+/0}$, which are 1.1−1.2 V less negative than that for [Ru(bpy)([14]aneS4)]$^{2+}$ (bpy = 2,2′-bipyridine). Both electrochemical data and DFT calculations suggest that the lowest unoccupied molecular orbitals of the nitrosated complexes are ON^N-centered. Natural population analysis shows that the amount of positive charge on the Ru centers and the [Ru([14]aneS4)] moieties in **2a** and **2b** is larger than that in [Ru(bpy)([14]aneS4)]$^{2+}$. According to the results of the structural, spectroscopic, electrochemical, and theoretical investigations, the ON^N ligands in this work have considerable π-acidic character and behave as better electron acceptors than bpy.

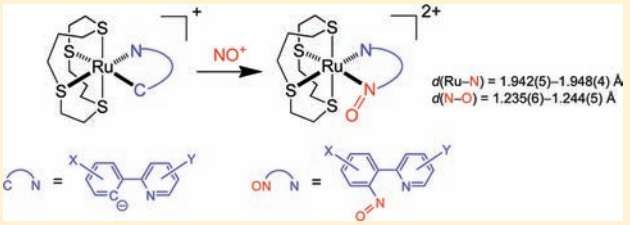

INTRODUCTION

The coordination chemistry of *C*-nitroso compounds (RN=O, R = alkyl or aryl) is of considerable interest from several perspectives. In the context of organic synthesis, *C*-nitroso compounds are attractive electrophiles in many C−N and/or C−O bond-forming reactions,[1−9] and investigations on the *C*-nitroso metal complexes provided useful results for the development of metal-mediated organic transformation reactions. Besides, the ability of nitrosoarenes to bind to the heme proteins like hemoglobin and myoglobin revealed their importance in various metabolic processes,[10−14] and this initiated a lot of studies on the electronic structures of metal nitrosoarene complexes.[15−23] Importantly, nitrosoarene ligands are redox-active,[24−27] and understanding the chemistry of metal nitrosoarene complexes can bring fundamental advances in inorganic and biological chemistry, although it has been recently pointed out by Wieghardt and co-workers that such rich redox activity has been largely overlooked in the literature.[28]

Our interest in the coordination chemistry of *C*-nitroso compounds stems from our recent discovery that a nitrosonium ion (NO$^+$) inserts into the Ru−aryl bond of 2-phenylpyridine anion (PhPy)-ligated ruthenium(II) complexes [Ru(PhPy)([9]aneS3)(L)]$^+$ ([9]aneS3 = 1,4,7-trithiacyclononane) to give 2-(2-nitrosophenyl)pyridine (NO-PhPy)-coordinated [Ru(NO-PhPy)([9]aneS3)(L)]$^{2+}$.[29] These NO-PhPy-ligated complexes represent the first structurally characterized transition-metal complexes bearing nitrosoarene with a pyridyl chelate, for which NO-PhPy behaves as a bidentate ligand via the two N atoms, with a bite angle close to 90°. Interestingly, the dihedral angles for the Ph/C−N−O plane pair and the Ph/Py pair in the crystal structure of [Ru(NO-PhPy)([9]aneS3)(CH$_3$CN)]$^{2+}$ are 36° and 26°, respectively, indicating that the pyridyl, phenyl, and NO moieties should, in principle, allow certain degrees of electron delocalization. We envision that comparing the structural, electrochemical, and spectroscopic properties of transition-metal complexes bearing 2-(2-nitrosoaryl)pyridine (denoted as ON^N) with their corresponding aromatic diimine analogues [like 2,2′-bipyridine (bpy)-ligated complexes] may yield interesting and important information regarding the metal−ON^N

Received: July 21, 2011
Published: October 24, 2011

bonding interaction in both the ground and excited states. We now present the preparation and structural, electrochemical, spectroscopic, and theoretical investigations of two series of ruthenium complexes containing ON^N and multidentate thioether ligands [9]aneS3 or 1,4,8,11-tetrathiacyclotetradecane ([14]aneS4). Our results suggest that the coordinated nitrosoarene on ON^N should be regarded as a neutral π-acid moiety $(ArNO)^0$ rather than monoanionic radical $(ArNO)^{\bullet-}$ or diamagnetic dianion $(ArNO)^{2-}$ and that the ON^N ligands are better electron acceptors than aromatic diimines.

RESULT AND DISCUSSION

Synthesis and Characterization. Nitroso complexes $[Ru(ON^N)([14]aneS4)]^{2+}$ (**2a**−**2d**) have been prepared in 60−80% yield by reacting the cyclometalated complexes **1a**−**1d** with $[NO][BF_4]$ (Scheme 1). The reaction proceeds smoothly to completion within 1 min at room temperature. This reactivity is the same as our recently reported insertion reaction of NO^+ into the Ru−C bond of the cyclometalated ruthenium(II) complex **3a** to give ON^N-ligated complex **4a**.[29] This is different from that for many ruthenium(II) complexes, which react with NO^+ substitutionally to give the ligand-substituted ruthenium nitrosyl compounds.[30−34] The [9]aneS3-isocyanide-ligated complexes **4a** and **4b** have also been prepared to compare the electron-donating/accepting ability of the ON^N ligands with aromatic diimines because the $\nu_{C\equiv N}$ value for $[Ru([9]aneS3)(phen)(C\equiv N^tBu)]^{2+}$ is available in the literature (2167 cm^{-1}).[35] The $\nu_{C\equiv N}$ values for complexes **4a** and **4b** (2188 and 2185 cm^{-1}, respectively) are larger than those for the phen-ligated analogues by ca. 20 cm^{-1}, revealing that the ON^N ligands are better electron acceptors than simple aromatic diimines. All of the ON^N-ligated complexes in this work have been found to be diamagnetic at room temperature, and the ν_{NO} values range from 1365 to 1396 cm^{-1}. These findings, together with the $Ru-N_{NO}$ and N−O distances of **2a** and **2b** (see the discussion below), suggest that the ON^N ligands in this work should be assigned as neutral $(ArNO)^0$ ligands rather than monoanionic radical $(ArNO)^{\bullet-}$ or diamagnetic dianion $(ArNO)^{2-}$ species.

Scheme 1

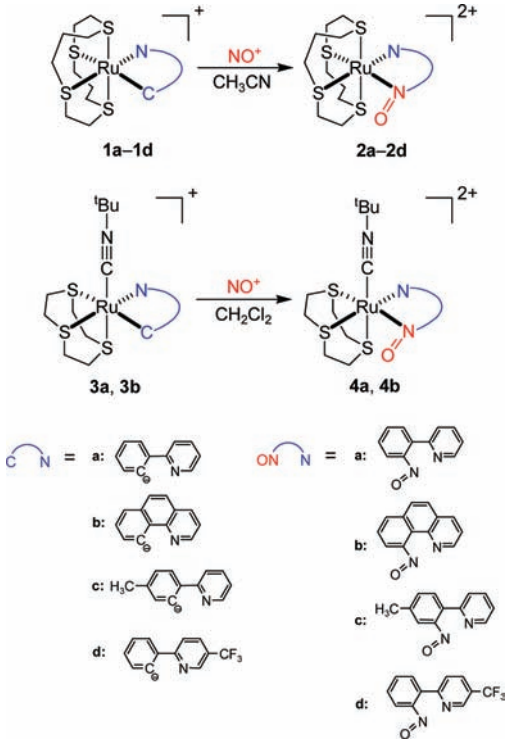

The crystal structures of complexes **1a**, **2a**, and **2b** have been determined by X-ray crystallography. Perspective views of their cations are depicted in Figure 1. Selected bond distances and angles are summarized in Table 1. In each case, the Ru atom adopts a cis-octahedral geometry. Disorder has been observed in the [14]aneS4 ligands for the cations in **2a** and **2b**, which are attributed to there being two possible ways that a [14]aneS4 coordinates to a *cis*-[Ru(X)(Y)] moiety (Scheme 2a). Although three possible isomers can arise from orientation of the lone pairs of the equatorial S atoms (Scheme 2b),[36] only ligand conformation **II** has been observed crystallographically in the complexes in this work.

In the ON^N-ligated complexes, the ON^N ligands behave as bidentate chelates via the two N atoms. The [Ru−NO−C] moieties are essentially planar, with the sum of the angles around the N_{NO} ranging from 359.7 to 360.0°, consistent with sp^2 hybridization at the N_{NO} atoms. The $Ru-N_{NO}$ distances [1.942(5)−1.948(4) Å] are appreciably shorter than the $Ru-N_{Py}$ distances [2.1115(19)−2.141(4) Å], suggesting that the $Ru \rightarrow N_{NO}$ back-bonding interaction is stronger than that for $Ru \rightarrow N_{Py}$. On the other hand, the nitrosated aryl rings have a stronger trans influence than the pyridyl ring: Ru−S(trans to

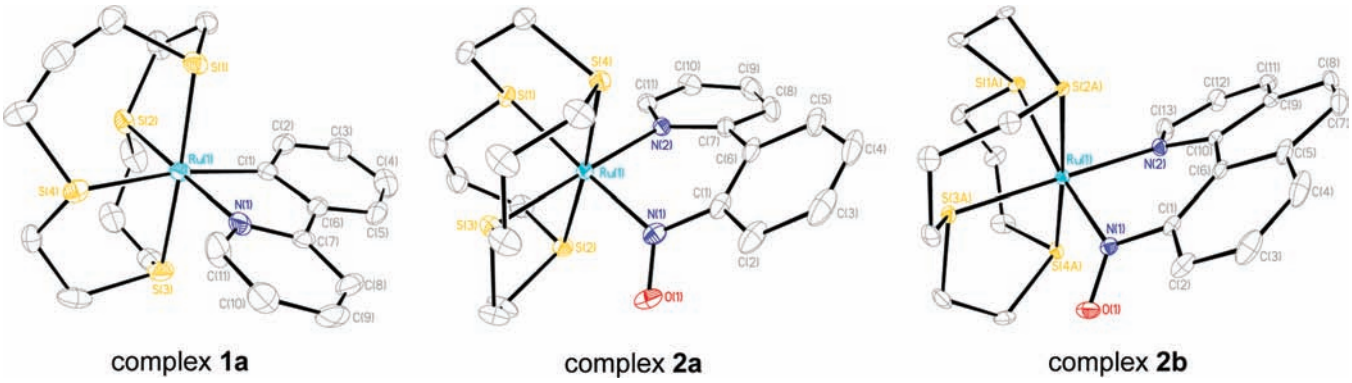

Figure 1. Perspective views of the cations in $\mathbf{1a}(ClO_4)$, $\mathbf{2a}(ClO_4)_2$, and $\mathbf{2b}(PF_6)_2 \cdot CH_3NO_2$. H atoms have been omitted for clarity. Thermal ellipsoids are at the 30% probability level.

dx.doi.org/10.1021/ic201570d |*Inorg. Chem.* 2011, 50, 11636–11643

Table 1. Selected Bond Lengths (Å) and Angles (deg) for 1a(ClO_4), 2a$(ClO_4)_2$, and 2b$(PF_6)_2\cdot CH_3NO_2$

	1a(ClO_4)	2a$(ClO_4)_2$[a]	2b$(PF_6)_2\cdot CH_3NO_2$
Ru−N_{NO}		1.948(4), 1.942(5)	1.9435(19)
Ru−N_{Py}	2.121(7)	2.141(4), 2.137(4)	2.1115(19)
N_{NO}−O		1.244(5), 1.235(6)	1.242(3)
Ru−C	2.077(9)		
N_{NO}−C		1.428(7), 1.442(7)	1.445(3)
Ru−S(trans to NO)		2.3928(12), 2.42[d]	2.40[d]
Ru−S(trans to Py)		2.3140(13), 2.3104(12)	2.33[d]
Ru−N−O		125.5(3), 126.9(4)	125.13(17)
Ru−N_{NO}−C		119.9(3), 119.9(4)	120.29(16)
O−N_{NO}−C		114.4(4), 113.1(5)	114.3(2)
N_{NO}−Ru−N_{Py}		87.83(16), 86.84(18)	87.19(8)
∠Py/Ar[b]	7.36	32.91, 25.58	15.52
∠Ar/C−N−O[c]		36.83, 36.37	27.22

[a] The crystal contains two crystallographically independent ruthenium complexes in the asymmetric unit. [b] The angle between the mean plane of the pyridyl ring and the cyclometalated aryl ring (for **1a**) or the nitrosated aryl ring (for **2a** and **2b**). [c] The angle between the mean plane of the nitrosated aryl ring and the plane constructed by the C, N, and O atoms. [d] The S atoms are disordered over two positions, and the Ru−S bond distances are weighted by the occupancy factors.

Scheme 2. (a) Two Possible Ways That a [14]aneS4 Coordinates to a *cis*-[Ru(X)(Y)] Moiety. (b) Three Possible Isomers That Arise from Orientation of the Lone Pairs of the Equatorial S Atoms

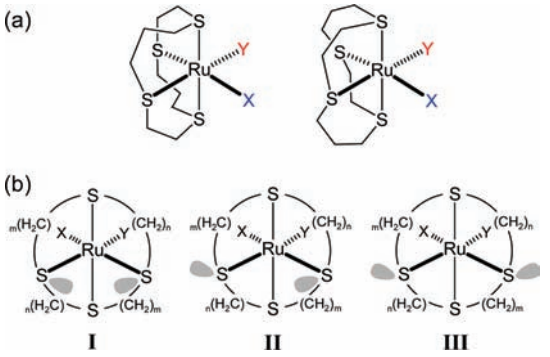

NO) and Ru−S(trans to Py) are 2.39−2.42 and 2.31−2.33 Å, respectively. The N_{NO}−O bond distances range from 1.235(6) to 1.244(5) Å, which is indicative of N−O double-bond character. These values are also comparable to those of other literature-reported ruthenium(II) complexes with nitrosoarene.[22,37] It is known that nitrosoarene may coordinate to a metal center as a neutral $(ArNO)^0$ ligand, monoanionic radical $(ArNO)^{\bullet-}$, or diamagnetic dianion $(ArNO)^{2-}$.[28] On the basis of the Ru−N_{NO} and N−O distances, the coordinated nitrosoarene in ON^N in this work should be assigned as a neutral species.

The bite angles for ON^N are 86.84(18)−87.83(16)°, which are comparable to that in [Ru(NO-PhPy)([9]aneS3)(CH_3CN)]$^{2+}$ [87.27(8)°].[29] It is also noted that the dihedral angles for the aryl/C−N−O plane pair and the aryl/Py pair are 27.2−36.8° and 15.5−32.9°, respectively, suggesting that electronic delocalization over the whole ON^N unit is possible. This is also supported by density functional theory (DFT) calculations (see the discussion below).

UV−Visible Absorption Studies. The UV−visible spectral data of all of the complexes are summarized in Table 2, and the absorption spectra of selected complexes are depicted in Figure 2. All complexes exhibit intense absorption at $\lambda_{max} \leq 300$ nm ($\varepsilon_{max} \geq 10^4$ dm^3 mol^{-1} cm^{-1}). Cyclometalated complexes **1a**−**1d** display moderately intense absorption centered at 384−416 nm [$\varepsilon_{max} = (4-6) \times 10^3$ dm^3 mol^{-1} cm^{-1}], whereas nitrosated complexes **2a**−**2d** show moderately intense absorption centered at 463−484 nm [$\varepsilon_{max} = (5-6) \times 10^3$ dm^3 mol^{-1} cm^{-1}] and a clearly discriminable absorption shoulder around 620 nm ($\varepsilon_{max} = (6-9) \times 10^2$ dm^3 mol^{-1} cm^{-1}), which tails up to 800 nm. Although the impact of the substituent on the pyridyl and nitrosated phenyl rings upon the absorption bands in the visible region is not dramatic, the absorption bands should contain some $Ru^{II} \rightarrow$ ON^N metal-to-ligand charge-transfer (MLCT) character because the peak maximum red-shifts in energy as the metal core changes from [Ru([9]aneS3)(C≡N^{t}Bu)] to [Ru([14]aneS4)] (442 nm for **4a** and 463 nm for **2a**) and as the conjugation of ON^N increases (463 nm for **2a**, 484 nm for **2b**, 442 nm for **4a**, and 460 nm for **4b**). In line with this argument, time-dependent DFT (TD-DFT) calculations suggest the visible absorption for **2a** and **2b** to be a mixing of d(Ru) → ON^N MLCT and ON^N intraligand (IL) transitions (see the discussion below).

It is noted that the $Ru^{II} \rightarrow$ ON^N MLCT transition energies are red-shifted by at least 3000 cm^{-1} compared with that for the $Ru^{II} \rightarrow$ bpy MLCT transition in [Ru(bpy)([14]aneS4)]$^{2+}$ ($\lambda_{max} = 401$ nm). A similar finding has also been observed during a comparison of the MLCT transition energies for **4a** and **4b** with their aromatic diimine analogue ([Ru(phen)([9]aneS3)-(C≡N^{t}Bu)]$^{2+}$ ($\lambda_{max} = 388$ nm). All of these results suggest that the ON^N ligand, even not in a perfectly coplanar configuration, features a lower-energy π^* molecular orbital (MO) than the nearly coplanar aromatic diimines. This is likely attributed to involvement of the low-lying π^* of the [N═O] moiety in the π system of the ON^N ligands.

Cyclic Voltammetry. Cyclic voltammetry has been used to examine the electrochemistry of all of the complexes in this work (Table 3; all values vs $Cp_2Fe^{+/0}$). No oxidation wave has been observed for the nitrosated complexes **2a**−**2d**, **4a**, and **4b** within the solvent window (solvent = CH_3CN), and their first reduction couples range from −0.53 to −0.62 V. Because the first reduction couples are sensitive to a change of the substituents on both

dx.doi.org/10.1021/ic201570d |*Inorg. Chem.* 2011, 50, 11636–11643

Table 2. UV−Visible Absorption Data[a]

complex	λ_{max}/nm (ε/dm^3 mol^{-1} cm^{-1})
1a	253 (18 570), 284 (19 180), 384 (5390)
1b	258 (30 480), 303 (sh, 7060), 349 (6270), 397 (5410)
1c	254 (19 220), 284 (22 850), 378 (6060)
1d	258 (15 200), 297 (17 160), 350 (sh, 2690), 416 (4710)
2a	238 (24 970), 289 (13 440), 320 (sh, 7330), 463 (5860), 610 (sh, 570)
2b	266 (23 800), 325 (10 170), 484 (5610), 612 (sh, 980)
2c	238 (sh, 25 340), 258 (sh, 19 590), 295 (16 460), 416 (sh, 4070), 470 (6130), 612 (sh, 630)
2d	236 (sh, 25 690), 267 (15 400), 294 (sh, 12 640), 326 (sh, 8700), 468 (5800), 618 (sh, 620)
3a	244 (19 220), 277 (17 630), 332 (sh, 3900), 380 (2450)
3b	255 (34 330), 286 (sh, 9870), 337 (8200), 404 (2820)
4a	232 (sh, 16 660), 253 (13 790), 285 (12 820), 390 (sh, 2970), 442 (4520)
4b	262 (31 530), 320 (13 710), 391 (4120), 460 (6670), 510 (sh, 4640)
[Ru(bpy)([14]aneS4)](PF$_6$)$_2$	243 (9080), 279 (19 830), 299 (sh, 10 010), 317 (7720), 401 (3770)

[a] Solvent = CH_3CN; temperature = 298 K.

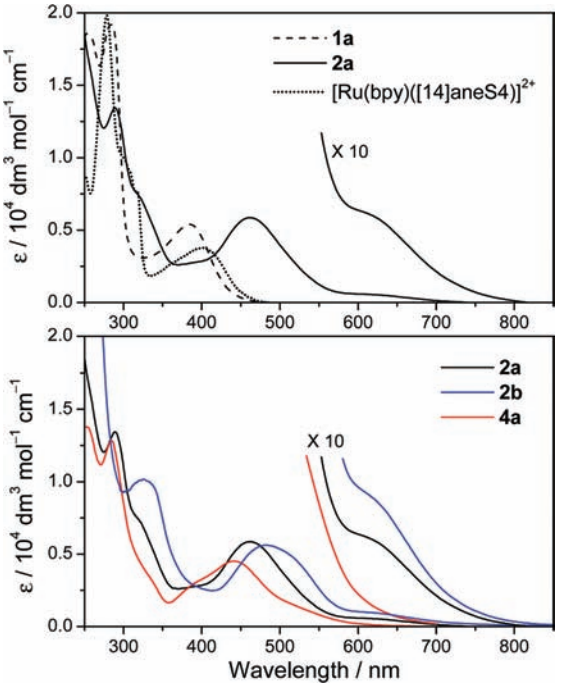

Figure 2. UV−visible absorption spectra of **1a**, **2a**, **2b**, **4a**, and [Ru([14]aneS4)(bpy)]$^{2+}$ in CH_3CN at 298 K.

the pyridyl and nitrosated aryl rings of the ON^N ligands, the lowest unoccupied molecular orbitals (LUMOs) of the nitrosated complexes may contain a contribution from the ON^N ligand. This is in agreement with our DFT calculations in which the LUMOs of these complexes are ON^N-centered (see the discussion below). It is noted that the first reduction potentials for **2a**−**2d** are 1.1−1.2 V less negative than that for [Ru(bpy)([14]aneS4)]$^{2+}$ (−1.72 V), and this is well-predicted by DFT calculations: the energies of the LUMOs of **2a** and **2b** are calculated to be 1 eV lower than that of [Ru(bpy)([14]aneS4)]$^{2+}$. For the cyclometalated complexes, the $E_{1/2}$ values for the first oxidation couples are 0.40−0.49 V for the [14]aneS4-ligated **1a**−**1d**, which are less positive than those for the [9]aneS3-isocyanide-supported counterparts (0.67−0.68 V for **3a**−**3b**).

Table 3. Electrochemical Data[a]

	$E_{1/2}$[b]/V vs $Cp_2Fe^{+/0}$		
complex	oxidation	first reduction	second reduction
1a	0.40		
1b	0.43	−2.40[c]	
1c	0.40		
1d	0.49	−2.31[c]	
2a		−0.61	−1.66
2b		−0.62	−1.48
2c		−0.62	−1.63[c]
2d		−0.53	−1.49
3a	0.68		
3b	0.67	−2.36[c]	
4a		−0.62	−1.63
4b		−0.59	−1.57
[Ru([14]aneS4)(bpy)]$^{2+}$	1.13	−1.72	

[a] Supporting electrolyte: 0.1 M [Bu_4N]PF_6 in CH_3CN. [b] $E_{1/2} = (E_{pc} + E_{pa})/2$ at 298 K for reversible couples. [c] Irreversible; the recorded potential is the cathodic potential at a scan rate of 100 mV s^{-1}.

Theoretical Calculations. DFT calculations have been performed on **2a**, **2b**, and [Ru(bpy)([14]aneS4)]$^{2+}$. The ground-state, gas-phase structures of these complexes have been optimized at the DFT level (B3LYP).[38,39] The ECP28MDF pseudopotential has been employed for Ru atoms with the correlation-consistent cc-pVTZ-PP basis set of Peterson et al.[40] and the 6-31+G* basis set for C, H, N, O, and S atoms.[41] The optimized structures have been confirmed to be local minima by frequency calculations. Detailed optimized structural data are summarized in the Supporting Information. The DFT-optimized structures for the calculated complexes are similar to their experimental structures. For example, the calculated Ru−N_{NO} and N−O bond distances and the bite angles of ON^N are 1.97 and 1.24 Å and 87° for **2a** and **2b**, which are comparable to their experimental values [1.942(5)−1.948(4) Å, 1.235(6)−1.244(5) Å, and 86.84(18)−87.83(16)° respectively]. Figure 4 depicts the optimized structures and the frontier MO surfaces of **2a** and **2b**. Table 4 summarizes the compositions

dx.doi.org/10.1021/ic201570d |Inorg. Chem. 2011, 50, 11636–11643

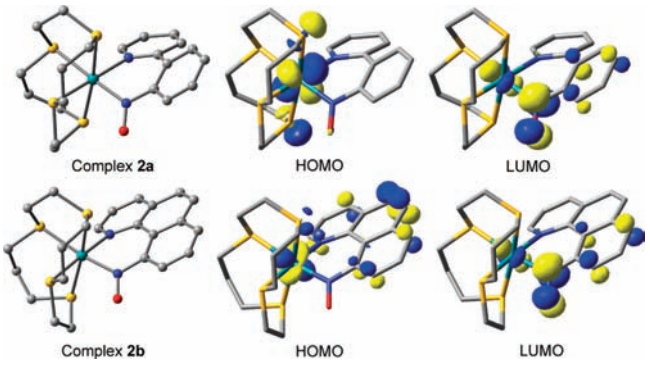

Figure 4. Optimized structures for **2a** and **2b** and their frontier MO surfaces (surface isovalue = 0.06 au) from TD-DFT calculations (gas phase).

Table 4. MO Compositions (%) of 2a and 2b in the Gas Phase and CH_3CN at the DFT-B3LYP-Optimized Geometry

complex	MO	s,p(Ru)	d(Ru)	ON^N	[14]aneS4
2a (gas phase)	HOMO	2.17	25.68	49.46	22.69
	LUMO	22.47	3.03	59.18	15.31
2b (gas phase)	HOMO	6.66	17.58	50.68	25.07
	LUMO	18.61	3.29	61.79	16.31
2a (CH_3CN)	HOMO−5	9.30	2.32	75.59	12.79
	HOMO−4	37.00	1.06	53.77	8.16
	HOMO−3	18.43	14.41	50.43	16.72
	HOMO−2	3.43	24.29	60.82	11.47
	HOMO−1	17.28	32.79	15.27	34.65
	HOMO	2.98	25.37	51.15	20.48
	LUMO	18.15	3.24	61.31	17.29
2b (CH_3CN)	HOMO−5	34.06	5.74	50.97	9.22
	HOMO−4	19.53	5.22	51.16	24.07
	HOMO−3	25.13	19.45	42.87	12.55
	HOMO−2	13.42	12.94	57.91	15.73
	HOMO−1	14.52	41.24	16.10	28.14
	HOMO	10.09	24.87	36.20	28.83
	LUMO	15.40	3.31	65.50	15.79

of the MOs that are of spectroscopic importance (see the discussion below). Although both the highest occupied molecular orbitals (HOMOs) and LUMOs of **2a** and **2b** are delocalized on the whole complexes, the HOMOs contain more d(Ru) character than the LUMOs, and the LUMOs are dominated by ON^N (ca. 60%).

The vertical electronic transitions for the calculated complexes have been investigated by the TD-DFT method with the conductor polarizable continuum model (CPCM) to account for solvent effects upon the electronic transition (solvent = CH_3CN). Calculated excitation energies, oscillator strengths, and absorption spectra constructed by convolution of these calculated transitions with Gaussian functions are depicted in Figure 5. The profiles of the convoluted absorption spectra are similar to those observed experimentally, i.e., moderately intense absorption around 500 nm with an absorption shoulder around 600 nm. For clarity, only the calculated vertical transition energies in the visible region are summarized in Table 5. The calculations show two types of one-electron excitation in the visible region: type 1, lower-energy transitions (ca. 500−600 nm) with oscillator strengths of 10^{-3}, which mainly arise

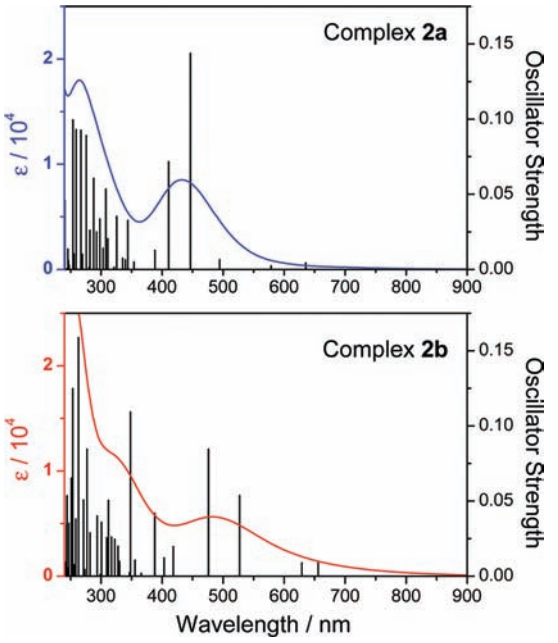

Figure 5. Calculated absorption spectra for **2a** and **2b** from TD-DFT/CPCM calculations. Excitation energies and oscillator strengths are shown by the black vertical lines; the spectra (in blue and red) are convoluted with a Gaussian function having full width at half-maximum of 0.33 eV.

from HOMO−1 → LUMO and HOMO → LUMO transitions; type 2, higher-energy transitions (ca. 400−500 nm) with oscillator strengths of 10^{-2}−10^{-1}, which originate from a combination of HOMO−X → LUMO transitions (X = 2−10). It is noted that in each complex the HOMO−1 and HOMO have higher d(Ru) contributions (25−41%) than that in the LUMO (3%), whereas the LUMO is dominated by ON^N (61−66%); therefore, type 1 transition contains d(Ru) → ON^N MLCT character. However, the contributions of ON^N in the HOMO−1 and HOMO are not low (15−51%), and this suggests that type 1 transitions also contain some ON^N IL character. HOMO−X are mostly dominated by ON^N (generally >50%) with a nonneglectable d(Ru) contribution, and thus the type 2 transitions are dominated by ON^N IL transitions but with some d(Ru) → ON^N MLCT component.

Although the formal oxidation state for the Ru centers in **2a**, **2b**, and $[Ru(bpy)([14]aneS4)]^{2+}$ is 2+, their partial charges calculated by natural population analysis (NPA)[42] are much lower because of the ligand-to-metal donation (Table 6). It is noted that the amount of positive charge on the Ru centers and the [Ru([14]aneS4)] moieties in **2a** and **2b** is larger than that in $[Ru(bpy)([14]aneS4)]^{2+}$, suggesting that ON^N is a better electron acceptor than bpy.

CONCLUSION

Two series of ruthenium complexes containing 2-(2-nitrosoaryl)pyridine (ON^N) have been prepared by insertion of a nitrosonium ion into the Ru−aryl bond of the corresponding cyclometalated ruthenium(II) complexes. The Ru−ON^N bonding interaction has been studied by structural, electrochemical, spectroscopic, and theoretical investigations. The ON^N ligands behave as bidentate chelates via the two N atoms, and the short Ru−N_{NO} distances [1.942(5)−1.948(4) Å] in **2a** and **2b**

dx.doi.org/10.1021/ic201570d |*Inorg. Chem.* 2011, 50, 11636–11643

Table 5. Calculated Vertical Transition Energies in the Visible Region for 2a and 2b at the TD-DFT/CPCM Level

		TD-DFT calculations	
complex	experimental λ_{max}/cm^{-1} ($\varepsilon_{max}/dm^3\ mol^{-1}\ cm^{-1}$)	excitation energy/cm^{-1} (oscillator strength)	composition of the excited-state wave functions
2a	16 390 (sh, 570)	15 730 (0.0043)	$0.63\ \Psi_{H\rightarrow L} - 0.29\ \Psi_{H-1\rightarrow L}$
		17 280 (0.0024)	$0.49\ \Psi_{H-1\rightarrow L} - 0.33\ \Psi_{H-2\rightarrow L} - 0.28\ \Psi_{H-3\rightarrow L} + 0.22\ \Psi_{H\rightarrow L}$
	21 600 (5860)	20 230 (0.0065)	$0.54\ \Psi_{H-4\rightarrow L} - 0.29\ \Psi_{H-3\rightarrow L} - 0.22\ \Psi_{H-1\rightarrow L} - 0.15\ \Psi_{H-5\rightarrow L} + 0.12\ \Psi_{H-9\rightarrow L}$
		22 400 (0.1438)	$0.61\ \Psi_{H-2\rightarrow L} + 0.27\ \Psi_{H-1\rightarrow L} + 0.17\ \Psi_{H\rightarrow L}$
		24 340 (0.0716)	$0.55\ \Psi_{H-3\rightarrow L} + 0.36\ \Psi_{H-4\rightarrow L} + 0.18\ \Psi_{H-1\rightarrow L}$
2b	16 340 (sh, 980)	15 240 (0.0088)	$0.51\ \Psi_{H-1\rightarrow L} + 0.46\ \Psi_{H\rightarrow L} + 0.11\ \Psi_{H-2\rightarrow L}$
		15 890 (0.0088)	$0.41\ \Psi_{H-1\rightarrow L} - 0.40\ \Psi_{H\rightarrow L} - 0.27\ \Psi_{H-2\rightarrow L} - 0.25\ \Psi_{H-3\rightarrow L} - 0.12\ \Psi_{H-4\rightarrow L}$
	20 660 (5610)	18 970 (0.0537)	$0.32\ \Psi_{H-3\rightarrow L} + 0.30\ \Psi_{H-5\rightarrow L} + 0.29\ \Psi_{H-2\rightarrow L} - 0.26\ \Psi_{H\rightarrow L} + 0.25\ \Psi_{H-4\rightarrow L} + 0.21\ \Psi_{H-1\rightarrow L} - 0.11\ \Psi_{H-10\rightarrow L} - 0.10\ \Psi_{H-6\rightarrow L}$
		21 000 (0.0846)	$0.52\ \Psi_{H-2\rightarrow L} - 0.32\ \Psi_{H-5\rightarrow L} - 0.22\ \Psi_{H-4\rightarrow L} - 0.20\ \Psi_{H\rightarrow L}$
		23 900 (0.0197)	$0.49\ \Psi_{H-4\rightarrow L} - 0.47\ \Psi_{H-3\rightarrow L} + 0.13\ \Psi_{H-2\rightarrow L}$

Table 6. NPA-Derived Partial Charges for 2a, 2b, and $[Ru(bpy)([14]aneS4)]^{2+}$

	partial charge		$[Ru(bpy)([14]aneS4)]^{2+}$	
atom	**2a**	**2b**	atom	partial charge
Ru	−0.02	−0.01	Ru	−0.10
N_{NO}	+0.13	+0.12	N_{bpy}	−0.42, −0.44
N_{Py}	−0.44	−0.44		
S_{ax}	+0.44, +0.46	+0.44, +0.45	S_{ax}	+0.45, +0.46
S_{eq}	+0.39, +0.43	+0.39, +0.41	S_{eq}	+0.40, +0.45
O	−0.35	−0.38		
[Ru([14]aneS4)]	+1.62	+1.61	[Ru([14]aneS4)]	+1.50
ON^N	+0.38	+0.39	bpy	+0.50

suggest that the Ru → N_{NO} back-bonding interaction is substantial. On the basis of the structural studies and $\nu_{N=O}$, the coordinated nitrosoarene in ON^N in this work should be assigned as a neutral species $(ArNO)^0$ rather than monoanionic radical $(ArNO)^{\bullet-}$ or dianion $(ArNO)^{2-}$ species. The nitrosated complexes feature moderately intense absorption bands covering the whole visible region, and TD-DFT calculations reveal that the transitions are a mixture of d(Ru) → ON^N MLCT and ON^N IL transitions. NPA shows that the amount of positive charge on the Ru centers and the [Ru([14]aneS4)] moieties in **2a** and **2b** is larger than that in $[Ru(bpy)([14]aneS4)]^{2+}$, suggesting that ON^N ligands are better electron acceptors than simple aromatic diimines. Because the absorption spectra of the ON^N-ligated complexes cover the entire spectral visible region, we envision that the ON^N ligands may open opportunities for developing sensitizers for solar energy conversion. Moreover, the noninnocent behavior of ON^N would be of fundamental interest, and studies are currently underway to isolate the reduced form of the ON^N-ligated complexes.

EXPERIMENTAL SECTION

General Procedures. All reactions were performed under an argon atmosphere using standard Schlenk techniques unless otherwise stated. All reagents were used as received, and solvents for the reactions were purified by a PureSolv MD5 solvent purification system. $[Ru(bpy)([14]aneS4)](PF_6)_2$ and $[Ru(PhPy)(CH_3CN)_4](PF_6)$ were prepared according to literature procedures.[36,43] Other cyclometalated analogues $[Ru(C^N)(CH_3CN)_4](PF_6)$ were synthesized by the same method as that of $[Ru(PhPy)(CH_3CN)_4](PF_6)$. ^1H, $^1H-^1H$ COSY, and $^1H-^1H$ NOESY NMR spectra were recorded on a Bruker 400 DRX FT-NMR spectrometer. Peak positions were calibrated with solvent residue peaks as the internal standard. The ^1H NMR spectra acquired at 293 K for the nitrosated complexes **2a**−**2d** only show one set of signals, although there are two possible ways that [14]aneS4 coordinates to the [Ru(ON^N)] moiety (Scheme 2a). This is because the two conformations of [14]aneS4 upon coordination to the [Ru(ON^N)] moiety are interchangeable at 293 K. Variable-temperature ^1H NMR experiments (193−293 K) have been performed on **2c** to investigate the possibility of observing the fluxional behavior of [14]aneS4. One more set of signals starts to appear at 233 K in the aromatic region, but these two sets of signals are not well-resolved even at 193 K and hampered calculation of the fluxional barrier.

Electrospray ionization mass spectrometry (ESI-MS) was performed on a PE-SCIEX API 3000 triple quadrupole mass spectrometer. IR spectra were recorded as KBr plates on a Perkin-Elmer FTIR-1600 spectrophotometer. UV−visible spectra were recorded on a Shimadzu UV-1700 spectrophotometer. Elemental analyses were done on an Elementar Vario EL analyzer. Cyclic voltammetry was performed with a CH Instrument model 600C series electrochemical analyzer/workstation. All solutions were degassed with argon before experiments. An $Ag/AgNO_3$ (0.1 M in CH_3CN) electrode was used as the reference electrode, and the $E_{1/2}$ value of the ferrocenium/ferrocene couple $(Cp_2Fe^{+/0})$ measured in the same solution was used as the internal reference. The mass magnetic susceptibility (χ_g) of **2a** was measured by a Johnson Matthey magnetic susceptibility balance MSB-1.

Nitroso Complexes 2a−2d, 4a, and 4b. Excess $[NO][BF_4]$ (5-fold) were added to the cyclometalated precursors (ca. 0.1 g) in dry CH_3CN under argon at room temperature. The color changed from yellow to dark red immediately. The reactions were stirred at room temperature for 1 min. The resulting dark-red solutions were concentrated and precipitated by the addition of aqueous NH_4PF_6 or $NaClO_4$. (***Caution!*** *Perchlorate salts are potentially explosive and should be handled with care and in small amounts.*) The dark-red precipitates (orange-red for **4a**) were washed with water followed by absolute ethanol and diethyl ether and dried under vacuum. The solids were then recrystallized by the slow diffusion of Et_2O into nitromethane solutions to give dark-red crystals.

2a(ClO$_4$)$_2$. Yield: 0.111 g, 91%. Anal. Calcd for $Ru_1C_{21}H_{28}N_2S_4Cl_2O_9$: C, 33.51; H, 3.75; N, 3.72. Found: C, 33.40; H, 3.94; N, 3.88. ^1H NMR (400 MHz, $(CD_3)_2CO$): δ 2.14−2.21, 2.65−2.77,

dx.doi.org/10.1021/ic201570d |*Inorg. Chem.* 2011, 50, 11636−11643

Scheme 3. Labeling Scheme for H Atoms on ON^N in Complexes 2a−2d, 4a, and 4b

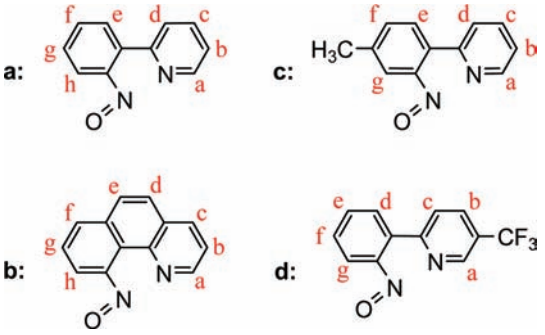

2.91−2.98, 3.23−3.49, 3.58−3.64, 3.87−3.99 (m, 20H, [14]aneS4), 7.49 (d, 1H, J = 7.9 Hz, H_h), 7.74−7.85 (m, 2H, H_b + H_g), 8.08 (t, 1H, J = 7.1 Hz, H_c/H_f), 8.41 (t, 1H, J = 7.2 Hz, H_f/H_c), 8.48 (d, 1H, J = 8.0 Hz, H_d/H_e), 8.56 (d, 1H, J = 8.2 Hz, H_e/H_d), 8.83 (d, 1H, J = 5.3 Hz, H_a). IR (KBr, cm^{-1}): $\nu_{N=O}$ 1374, ν_{Cl-O} 1084. ESI-MS: m/z 653 [M^{2+} + ClO_4^-].

2b(PF$_6$)$_2$. Yield: 0.081 g, 72%. Anal. Calcd for $Ru_1C_{23}H_{28}N_2S_4O_1P_2F_{12}\cdot CH_3NO_2$: C, 31.03; H, 3.36; N, 4.53. Found: C, 30.88; H, 3.52; N, 4.75. ^{1}H NMR (400 MHz, $(CD_3)_2CO$): δ 2.22−2.29, 2.60−2.71, 2.97−3.15, 3.28−3.45, 3.54−3.97, (m, 20H, [14]aneS4), 7.95 (d, 1H, J = 7.3 Hz, H_h), 8.07−8.12 (m, 2H, H_b + H_g), 8.36 (d, 1H, J = 8.8 Hz, H_d), 8.50 (d, 1H, J = 8.8 Hz, H_e), 8.82(d, 1H, J = 7.7 Hz, H_f), 9.02 (d, 1H, J = 8.0 Hz, H_c), 9.21 (d, 1H, J = 5.0 Hz, H_a). IR (KBr, cm^{-1}): $\nu_{N=O}$ 1381, ν_{P-F} 838. ESI-MS: m/z 723 [M^{2+} + PF_6^-].

2c(PF$_6$)$_2$. Yield: 0.100 g, 85%. Anal. Calcd for $Ru_1C_{22}H_{30}N_2S_4O_1P_2F_{12}\cdot CH_3NO_2$: C, 30.08; H, 3.62; N, 4.58. Found: C, 29.92; H, 3.56; N, 4.58. ^{1}H NMR (400 MHz, CD_3CN): δ 1.79−1.87, 2.36−2.43, 2.54−2.58, 2.89−3.09, 3.17−3.21, 3.31−3.41, 3.56−3.66 (m, 20H, [14]aneS4), 2.49 (s, 3H, CH_3 of ON^N), 7.05 (s, 1H, H_g), 7.63 (t, 1H, J = 6.1 Hz, H_b), 7.79 (d, 1H, J = 8.1 Hz, H_f), 8.14 (d, 1H, J = 8.1 Hz, H_e), 8.21 (t, 1H, J = 7.7 Hz, H_c), 8.27 (d, 1H, J = 8.8 Hz, H_d), 8.39 (d, 1H, J = 4.7 Hz, H_a). IR (KBr, cm^{-1}): $\nu_{N=O}$ 1365, ν_{P-F} 837. ESI-MS: m/z 713 [M^{2+} + PF_6^-].

2d(PF$_6$)$_2$. Yield: 0.093 g, 82%. Anal. Calcd for $Ru_1C_{22}H_{27}N_2S_4O_1P_2F_{15}\cdot CH_3NO_2$: C, 28.40; H, 3.11; N, 4.32. Found: C, 28.54; H, 3.21; N, 4.19. ^{1}H NMR (400 MHz, CD_3CN): δ 1.81−1.89, 2.40−2.67, 2.87−3.11, 3.19−3.23, 3.34−3.41, 3.57−3.72 (m, 20H, [14]aneS4), 7.27 (d, 1H, J = 7.4 Hz, H_g), 7.75 (t, 1H, J = 7.4 Hz, H_f), 8.02 (t, 1H, J = 7.3 Hz, H_e), 8.31 (d, 1H, J = 7.8 Hz, H_d), 8.48 (d, 1H, J = 8.6 Hz, H_c), 8.54 (d, 1H, J = 8.6 Hz, H_b), 8.60 (s, 1H, H_a). IR (KBr, cm^{-1}): $\nu_{N=O}$ 1379, ν_{P-F} 839. ESI-MS: m/z 766 [M^{2+} + PF_6^-].

4a(PF$_6$)$_2$. Yield: 0.082 g, 65%. Anal. Calcd for $Ru_1C_{22}H_{29}N_3S_3O_1P_2F_{12}$: C, 31.51; H, 3.48; N, 5.01. Found: C, 31.36; H, 3.67; N, 4.96. ^{1}H NMR (400 MHz, $(CD_3)_2CO$): δ 1.56 (s, 9H, ^{t}Bu), 2.43−2.52, 2.92−3.02, 3.05−3.11, 3.15−3.38, 3.58−3.74 (m, 12H, [9]aneS3), 7.30 (d, 1H, J = 7.1 Hz, H_h), 7.80−7.83 (m, 2H, H_b + H_g), 8.11 (t, 1H, J = 7.2 Hz, H_c/H_f), 8.39 (t, 1H, J = 7.2 Hz, H_f/H_c), 8.48 (d, 1H, J = 7.9 Hz, H_d/H_e), 8.55 (d, 1H, J = 8.1 Hz, H_e/H_d), 9.02 (d, 1H, J = 5.0 Hz, H_a). IR (KBr, cm^{-1}): $\nu_{C\equiv N}$ 2188, $\nu_{N=O}$ 1396, ν_{P-F} 834. ESI-MS: m/z 693 [M^{2+} + PF_6^-].

4b(ClO$_4$)$_2$. Yield: 0.086 g, 63%. Anal. Calcd for $Ru_1C_{24}H_{29}N_3S_3Cl_2O_9$: C, 37.35; H, 3.79; N, 5.45. Found: C, 37.62; H, 3.84; N, 5.50. ^{1}H NMR (400 MHz, CD_3CN): δ 1.52 (s, 9H, ^{t}Bu), 2.18−2.24, 2.36−2.45, 2.53−2.61, 2.74−2.80, 2.85−2.90, 3.06−3.16, 3.22−3.27, 3.42−3.47 (m, 12H, [9]aneS3), 7.59 (d, 1H, J = 7.8 Hz, H_h), 7.89−7.92 (m, 1H, H_b), 7.98 (t, 1H, J = 7.9 Hz, H_g), 8.18 (d, 1H, J = 8.8 Hz, H_d), 8.32 (d, 1H, J = 8.9 Hz, H_e), 8.66 (d, 1H, J = 7.9 Hz, H_f), 8.79 (dd, 1H, J = 8.1 and 1.1 Hz, H_c), 9.12 (dd, 1H, J = 5.4 and 1.3 Hz, H_a). IR (KBr, cm^{-1}): $\nu_{C\equiv N}$ 2185, $\nu_{N=O}$ 1370, ν_{Cl-O} 1080. ESI-MS: m/z 672 [M^{2+} + ClO_4^-].

X-ray Crystallography. X-ray diffraction data for **1a**(ClO_4), **2a**-(ClO_4)$_2$, and **2b**(PF_6)$_2\cdot CH_3NO_2$ were collected on an Oxford Diffraction Gemini S Ultra X-ray single-crystal diffractometer with Cu Kα radiation (λ = 1.541 78 Å) or Mo Kα radiation (λ = 0.710 73 Å) at 133 K. The data were processed using *CrysAlis*.[44] The structures were solved by Patterson and Fourier methods and refined by full-matrix least squares based on F^2 with programs *SHELXS-97* and *SHELXL-97*[45] within *WinGX*.[46] All non-H atoms were refined anisotropically in the final stage of least-squares refinement. The positions of H atoms were calculated based on the riding mode with thermal parameters equal to 1.2 times that of the associated C atoms. Disorder of the cations in **2a**(ClO_4)$_2$ and **2b**(PF_6)$_2\cdot CH_3NO_2$ was observed, which arises from there being two ways in which [14]andS4 can coordinate to the [Ru(ON^N)] moiety. Disorder of the anions in **2a**(ClO_4)$_2$ and **2b**-(PF_6)$_2\cdot CH_3NO_2$ was also observed. Split models and several DFIX and ISOR restraints were applied in the refinement of these crystal structures.

Computational Methodology. DFT calculations were performed on [Ru([14]aneS4)(bpy)]$^{2+}$, **2a**, and **2b**. Their electronic ground states were optimized without symmetry imposed using Becke's three-parameter hybrid functional with the Lee−Yang−Parr correlation functional (B3LYP).[38,39] The ECP28MDF pseudopotential was employed for the Ru atoms with the correlation-consistent cc-pVTZ-PP basis set of Peterson et al.[40] The 6-31+G* basis set was employed for C, H, N, O, and S atoms.[41] Tight self-consistent-field convergence (10^{-8}au) was used for all calculations. Frequency calculations were also performed on all of the optimized structures. Because no imaginary vibrational frequencies were encountered, the optimized stationary points were confirmed to be local minima. The vertical transition energies for **2a** and **2b** in CH_3CN were computed at their respective gas-phase-optimized ground-state geometries using the TD-DFT method with the same density functional and basis sets in the geometry optimizations. The CPCM[47] was used to account for solvent effects upon the electronic transition. NPA was performed using *NBO 3.0*[42] implemented to *Gaussian 03*. All of the calculations were performed using the *Gaussian 03* program package (revision D.01).[48]

■ ASSOCIATED CONTENT

Supporting Information. Synthetic procedures for cyclometalated complexes **1a**−**1d** and **3b**, optimized geometries for **2a**, **2b**, and [Ru([14]aneS4)(bpy)]$^{2+}$, plots of MO surfaces that are of spectroscopic importance for **2a** and **2b**, and CIF files. This material is available free of charge via the Internet at http://pubs.acs.org.

■ AUTHOR INFORMATION

Corresponding Author
*E-mail: acywong@cityu.edu.hk.

■ ACKNOWLEDGMENT

The work described in this paper was supported by a grant from City University of Hong Kong (Project 7002591). We are grateful to Dr. Shek-Man Yiu for X-ray diffraction data collection.

■ REFERENCES

(1) Kirby, G. W. *Chem. Soc. Rev.* **1977**, *6*, 1.
(2) Zuman, P.; Shah, B. *Chem. Rev.* **1994**, *94*, 1621.

(3) Momiyama, N.; Yamamoto, H. *Org. Lett.* **2002**, *4*, 3579.
(4) Adam, W.; Krebs, O. *Chem. Rev.* **2003**, *103*, 4131.
(5) Gowenlock, B. G.; Richter-Addo, G. B. *Chem. Rev.* **2004**, *104*, 3315.
(6) Gowenlock, B. G.; Richter-Addo, G. B. *Chem. Soc. Rev.* **2005**, *34*, 797.
(7) Yamamoto, H.; Momiyama, N. *Chem. Commun.* **2005**, 3514.
(8) Yamamoto, Y.; Yamamoto, H. *Eur. J. Org. Chem.* **2006**, 2031.
(9) Payette, J. N.; Yamamoto, H. *J. Am. Chem. Soc.* **2008**, *130*, 12276.
(10) Loeb, R. F.; Bock, A. V.; Fitz, R. *Am. J. Med. Sci.* **1921**, *161*, 539.
(11) Chottard, G.; Mansuy, D. *Biochem. Biophys. Res. Commun.* **1977**, *77*, 1333.
(12) Alston, T. A.; Porter, D. J. T.; Bright, H. J. *Acc. Chem. Res.* **1983**, *16*, 418.
(13) Kazanis, S.; McClelland, R. A. *J. Am. Chem. Soc.* **1992**, *114*, 3052.
(14) Stone, J. R.; Marletta, M. A. *Biochemistry* **1995**, *34*, 16397.
(15) Little, R. G.; Doedens, R. J. *Inorg. Chem.* **1973**, *12*, 537.
(16) Cameron, M.; Gowenlock, B. G. *Chem. Soc. Rev.* **1990**, *19*, 355.
(17) Wang, L.-S.; Chen, L.; Khan, M. A.; Richter-Addo, G. B. *Chem. Commun.* **1996**, 323.
(18) Fox, S. J.; Chen, L.; Khan, M. A.; Richter-Addo, G. B. *Inorg. Chem.* **1997**, *36*, 6465.
(19) Richter-Addo, G. B. *Acc. Chem. Res.* **1999**, *32*, 529.
(20) Godbout, N.; Sanders, L. K.; Salzmann, R.; Havlin, R. H.; Wojdelski, M.; Oldfield, E. *J. Am. Chem. Soc.* **1999**, *121*, 3829.
(21) Lee, J.; Chen, L.; West, A. H.; Richter-Addo, G. B. *Chem. Rev.* **2002**, *102*, 1019.
(22) Lee, J.; Twamley, B.; Richter-Addo, G. B. *Dalton Trans.* **2004**, 189.
(23) Labios, L. A.; Millard, M. D.; Rheingold, A. L.; Figueroa, J. S. *J. Am. Chem. Soc.* **2009**, *131*, 11318.
(24) Mansuy, D.; Battioni, P.; Chottard, J.-C.; Riche, C.; Chiaroni, A. *J. Am. Chem. Soc.* **1983**, *105*, 455.
(25) Rehorek, D. *Chem. Soc. Rev.* **1991**, *20*, 341.
(26) Iwasa, T.; Shimada, H.; Takami, A.; Matsuzaka, H.; Ishii, Y.; Hidai, M. *Inorg. Chem.* **1999**, *38*, 2851.
(27) Askari, M. S.; Girard, B.; Murugesu, M.; Ottenwaelder, X. *Chem. Commun.* **2011**, *47*, 8055.
(28) Tomson, N. C.; Labios, L. A.; Weyhermüller, T.; Figueroa, J. S.; Wieghardt, K. *Inorg. Chem.* **2011**, *50*, 5763.
(29) Chan, S.-C.; Pat, P.-K.; Lau, T.-C.; Wong, C.-Y. *Organometallics* **2011**, *30*, 1311.
(30) Efraty, A.; Elbaze, G. *J. Organomet. Chem.* **1984**, *260*, 331.
(31) Conroy-Lewis, F. M.; Redhouse, A. D.; Simpson, S. J. *J. Organomet. Chem.* **1990**, *399*, 307.
(32) Shaver, A.; El-khateeb, M.; Lebuis, A.-M. *Inorg. Chem.* **1995**, *34*, 3841.
(33) Diversi, P.; Fontani, M.; Fuligni, M.; Laschi, F.; Matteoni, S.; Pinzino, C.; Zanello, P. *J. Organomet. Chem.* **2001**, *626*, 145.
(34) Hadadzadeh, H.; DeRosa, M. C.; Yap, G. P. A.; Rezvani, A. R.; Crutchley, R. J. *Inorg. Chem.* **2002**, *41*, 6521.
(35) Wong, C.-Y.; Lai, L.-M.; Leung, H.-F.; Wong, S.-H. *Organometallics* **2009**, *28*, 3537.
(36) Adams, H.; Amado, A. M.; Félix, V.; Mann, B. E.; Antelo-Martinez, J.; Newell, M.; Ribeiro-Claro, P. J. A.; Spey, S. E.; Thomas, J. A. *Chem.—Eur. J.* **2005**, *11*, 2031.
(37) Liang, J.-L.; Huang, J.-S.; Zhou, Z.-Y.; Cheung, K.-K.; Che, C.-M. *Chem.—Eur. J.* **2001**, *7*, 2306.
(38) Becke, A. D. *J. Chem. Phys.* **1993**, *98*, 5648.
(39) Lee, C.; Yang, W.; Parr, R. G. *Phys. Rev. B* **1988**, *37*, 785.
(40) Peterson, K.; Figgen, D.; Dolg, M.; Stoll, H. *J. Chem. Phys.* **2007**, *126*, 124101.
(41) (a) Hehre, W. J.; Ditchfield, R.; Pople, J. A. *J. Chem. Phys.* **1972**, *56*, 2257. (b) Francl, M. M.; Pietro, W. J.; Hehre, W. J.; Binkley, J. S.; Gordon, M. S.; DeFrees, D. J.; Pople, J. A. *J. Chem. Phys.* **1982**, *77*, 3654.
(42) Reed, A. E.; Curtiss, L. A.; Weinhold, F. *Chem. Rev.* **1988**, *88*, 899.
(43) Fernandez, S.; Pfeffer, M.; Ritleng, V.; Sirlin, C. *Organometallics* **1999**, *18*, 2390.
(44) *CrysAlis*, version 1.171.31.8; Oxford Diffraction Ltd.: Oxford, U.K., 2007.
(45) Sheldrick, G. M. *SHELXS-97 and SHELXL-97, Program for Crystal Structure Solution and Refinements*; University of Göttingen: Göttingen, Germany, 1997.
(46) Farrugia, L. J. *J. Appl. Crystallogr.* **1999**, *32*, 837.
(47) Barone, V.; Cossi, M. *J. Phys. Chem. A* **1998**, *102*, 1995.
(48) Frisch, M. J.; Trucks, G. W.; Schlegel, H. B.; Scuseria, G. E.; Robb, M. A.; Cheeseman, J. R.; Montgomery, J. A., Jr.; Vreven, T.; Kudin, K. N.; Burant, J. C.; Millam, J. M.; Iyengar, S. S.; Tomasi, J.; Barone, V.; Mennucci, B.; Cossi, M.; Scalmani, G.; Rega, N.; Petersson, G. A.; Nakatsuji, H.; Hada, M.; Ehara, M.; Toyota, K.; Fukuda, R.; Hasegawa, J.; Ishida, M.; Nakajima, T.; Honda, Y.; Kitao, O.; Nakai, H.; Klene, M.; Li, X.; Knox, J. E.; Hratchian, H. P.; Cross, J. B.; Bakken, V.; Adamo, C.; Jaramillo, J.; Gomperts, R.; Stratmann, R. E.; Yazyev, O.; Austin, A. J.; Cammi, R.; Pomelli, C.; Ochterski, J. W.; Ayala, P. Y.; Morokuma, K.; Voth, G. A.; Salvador, P.; Dannenberg, J. J.; Zakrzewski, V. G.; Dapprich, S.; Daniels, A. D.; Strain, M. C.; Farkas, O.; Malick, D. K.; Rabuck, A. D.; Raghavachari, K.; Foresman, J. B.; Ortiz, J. V.; Cui, Q.; Baboul, A. G.; Clifford, S.; Cioslowski, J.; Stefanov, B. B.; Liu, G.; Liashenko, A.; Piskorz, P.; Komaromi, I.; Martin, R. L.; Fox, D. J.; Keith, T.; Al-Laham, M. A.; Peng, C. Y.; Nanayakkara, A.; Challacombe, M.; Gill, P. M. W.; Johnson,B.; Chen,W.; Wong, M. W.; Gonzalez, C.; Pople, J. A. *Gaussian 03*, revision D.01; Gaussian, Inc.: Wallingford, CT, 2004.